GEOCHEMISTRY

Lithium isotopic constraints on the evolution of continental clay mineral factory and marine oxygenation in the earliest Paleozoic Era

Guang-Yi Wei[1,2]*, Mingyu Zhao[3,2]*, Erik A. Sperling[4], Robert R. Gaines[5], Boriana Kalderon-Asael[2], Jun Shen[6], Chao Li[7,8,9], Feifei Zhang[1], Gaojun Li[1], Chuanming Zhou[10], Chunfang Cai[3], Daizhao Chen[3], Ke-Qing Xiao[11,12], Lei Jiang[3], Hong-Fei Ling[1], Noah J. Planavsky[2], Lidya G. Tarhan[2]

The evolution of oxygen cycles on Earth's surface has been regulated by the balance between molecular oxygen production and consumption. The Neoproterozoic–Paleozoic transition likely marks the second rise in atmospheric and oceanic oxygen levels, widely attributed to enhanced burial of organic carbon. However, it remains disputed how marine organic carbon production and burial respond to global environmental changes and whether these feedbacks trigger global oxygenation during this interval. Here, we report a large lithium isotopic and elemental dataset from marine mudstones spanning the upper Neoproterozoic to middle Cambrian [~660 million years ago (Ma) to 500 Ma]. These data indicate a dramatic increase in continental clay formation after ~525 Ma, likely linked to secular changes in global climate and compositions of the continental crust. Using a global biogeochemical model, we suggest that intensified continental weathering and clay delivery to the oceans could have notably increased the burial efficiency of organic carbon and facilitated greater oxygen accumulation in the earliest Paleozoic oceans.

INTRODUCTION

Although photosynthetic production of oxygen emerged early in Earth's history [~3.0 billion years ago (Ga)], increases in atmospheric and marine reservoirs of oxygen, linked to fundamental shifts in the source-sink balance of molecular oxygen, were substantially delayed (*1*–*3*). The stepwise oxygenation of Earth's surface environments following the emergence of oxygenic photosynthesis, such as the Great Oxidation Event (GOE), occurring around 2.4 to 2.1 Ga, and the Neoproterozoic Oxygenation Event (NOE), spanning ~0.8 Ga to 0.55 Ga, was ultimately caused by elevated production or reduced consumption of molecular oxygen (*4*, *5*). Before the rise of land plants, the transfer and burial of photosynthetically produced marine organic carbon (OC) from the surface ocean to seafloor sediments (i.e., the marine biological carbon pump) likely served as the primary source of molecular oxygen to the Earth's surface over million-year timescales (*6*). Secular changes in OC production and burial are closely related to shifts in biological evolution, global tectonics, and biogeochemical cycles (*2*, *5*, *7*). Increases in the availability of nutrients (e.g., phosphorus) and the emergence of new clades of primary producers in the oceans are assumed to have intensified the biological pump and OC burial over time and thus to have driven the rise of atmospheric and oceanic O_2 levels (*7*–*9*). In today's oceans, only a small fraction of OC reaching the seafloor (<0.03 to 13%) will ultimately be buried, while a far larger portion is broken down by microbial respiration (*10*, *11*). Therefore, factors regulating OC burial efficiency in marine sediments may have played a critical role in shaping global redox landscapes throughout Earth's history. The late Neoproterozoic to early Paleozoic is considered to mark a second major increase in atmospheric O_2 levels (*4*, *12*), although the overall extent of global atmospheric and oceanic oxygenation during this interval may still have been limited relative to the modern Earth (*13*–*16*). However, the identification of drivers of secular shifts in OC burial and the oxygenation of the oceans and atmosphere remains contentious from the late Neoproterozoic to the early Paleozoic (*2*, *17*–*21*).

Myriad factors are proposed to influence OC burial efficiency in marine sediments, including sedimentation rates, seawater chemistry, temperature, the biochemical reactivity of organic particles, and mineral protection (i.e., interactions between OC and mineral matrices, protecting OC from oxidation by means of sorption or inhibition of microbial decay) (*11*, *21*–*24*). Mineral protection, in particular, plays a strong role in shaping the fate of OC in modern seafloor sediments (*25*–*28*), particularly via binding with clays (*29*–*31*). Therefore, associations between seafloor mineral assemblages and OC burial may be closely related to the geological oxygen cycle and to past oceanic redox states (*19*, *32*, *33*). Previous studies have proposed that enhanced orogenesis related to Gondwana amalgamation and subsequently accelerated chemical weathering could have enhanced the marine burial of OC in the late Neoproterozoic (*19*, *34*). However, empirical evidence

[1]School of Earth Sciences and Engineering, and Frontiers Science Center for Critical Earth Material Cycling, Nanjing University, Nanjing 210023, China. [2]Department of Earth and Planetary Sciences, Yale University, New Haven, CT 06520-8109, USA. [3]Key Laboratory of Cenozoic Geology and Environment, Institute of Geology and Geophysics, Chinese Academy of Sciences, Beijing, China. [4]Department of Earth and Planetary Sciences, Stanford University, Stanford, CA 94305, USA. [5]Geology Department, Pomona College, Claremont, CA 91711, USA. [6]State Key Laboratory of Geological Processes and Mineral Resources, China University of Geosciences, Wuhan 430074, China. [7]State Key Laboratory of Oil and Gas Reservoir Geology and Exploitation and Institute of Sedimentary Geology, Chengdu University of Technology, Chengdu 610059, China. [8]Key Laboratory of Deep-time Geography and Environment Reconstruction and Applications of Ministry of Natural Resources, Chengdu University of Technology, Chengdu 610059, China. [9]International Center for Sedimentary Geochemistry and Biogeochemistry Research, Chengdu University of Technology, Chengdu 610059, China. [10]State Key Laboratory of Palaeobiology and Stratigraphy, Nanjing Institute of Geology and Palaeontology, and Center for Excellence in Life and Palaeoenvironment, Chinese Academy of Sciences, Nanjing 210008, China. [11]State Key Lab of Urban and Regional Ecology, Research Center for Eco-Environmental Sciences, Chinese Academy of Sciences, Shuangqing Rd. 18, 10085, Beijing, China. [12]University of Chinese Academy of Sciences, Beijing, 100049, China.
*Corresponding author. Email: guangyiwei@nju.edu.cn (G.-Y.W.); mingyu.zhao@mail.iggcas.ac.cn (M.Z.)

for this feedback and clear links between shifts in the continental clay factory and global oxygenation have hitherto been limited.

Here, we report a large ($n = 550$) dataset of lithium isotope (δ^7Li) and K/Al ratios from marine fine-grained siliciclastic rocks (i.e., mudstones) from Canada, the United States, Namibia, the Tarim Basin (NW China), and South China, spanning the upper Neoproterozoic to the middle Cambrian [~660 million years ago (Ma) to 500 Ma] (fig. S1). We assess these data with the aim of reconstructing secular trends in the distribution of marine sedimentary clay and continental silicate weathering patterns over this critical time interval. These data reveal substantial increases in the production of continental clay, concurrent with increases in the OC and uranium content of fine-grained siliciclastic rocks, beginning in the early Cambrian (~525 Ma). We interpret these results to be a signal for intensified continental silicate weathering and continental clay delivery to the continental shelves during the early Cambrian, which would have promoted the burial and preservation of OC in marine sediments and thus facilitated increases in oxygen accumulation in the earliest Paleozoic oceans.

Lithium isotope of marine mudstones as a tracer for continental clay formation

Fined-grained marine siliciclastic rocks generally consist of a combination of products from continental physical erosion (unweathered rock fragments and primary minerals), continental chemical weathering (continentally formed clays), along with marine reverse weathering (authigenic clays precipitated into seafloor sediments) (*35*). Siliciclastic sediments on continental shelves are dominated by-products of continental physical and chemical weathering due to high detrital sedimentation rates (*36*, *37*), with substantial local variation in the relative proportions of clay minerals to unweathered rock fragments and primary minerals (e.g., mica, feldspar, and quartz) controlled by tectonics- and climate-mediated differences in weatherability in source areas (*38*, *39*). Continental detrital materials (e.g., mica, feldspar, and smectite) can also be transformed into new clay minerals during depositional and early diagenetic processes on the continental shelf, and some clay minerals (e.g., chlorites) can be derived through either continental weathering or marine authigenesis (*40*–*43*). In addition, due to elevated rates of reverse weathering (*37*), the accumulation of authigenic clays in Neoproterozoic and early Paleozoic marine sediments may have been greater than in the modern ocean, potentially diluting continental weathering products and further hampering their identification in marine mudstones. Distinguishing between marine authigenic clays, continental clays, and unweathered primary silicates within ancient sedimentary successions through conventional petrographic and mineralogical analyses has proven challenging. Lithium isotopes represent a promising tool to explore the extent of continental clay contribution to marine siliciclastic sediments, as clay minerals preferentially incorporate the lighter Li isotope (^{6}Li) relative to upper crustal materials (*44*–*47*). Continentally formed clays and marine authigenic clays can also exhibit distinct δ^7Li signatures as a result of large expected δ^7Li differences between their precipitating fluids (*48*–*49*). Under steady-state conditions with respect to the global marine Li cycle, seawater δ^7Li reflects a balance between all input and removal fluxes and their isotopes. Therefore, δ^7Li values of marine authigenic clays, which were likely the predominant sink for seawater Li during the Precambrian (*50*), are likely to be roughly equal to the average δ^7Li value of Li sources to the ocean (i.e., the weighted average of the δ^7Li values of river waters and hydrothermal fluids) and potentially distinctly higher than those of continental clays and unweathered primary silicate minerals (*51*–*53*). Substantial continental clay formation during chemical weathering, on the other hand, can be distinguished by notably negative δ^7Li values, associated with incongruent weathering of primary silicate minerals, given that the average δ^7Li value of the upper continental crust (UCC) is roughly 0‰ (per mil) (*38*, *54*, *55*). Today, rock provenance and silicate weathering intensity are likely the primary levers on the δ^7Li values of riverine detrital materials delivered to the oceans (*38*, *55*). Studies of modern river sediments suggest that modern continental denudation is cannibalistic, and δ^7Li signatures of detrital materials are fundamentally controlled by newly formed weathering products (enriched in the light Li isotope relative to bedrock) and unweathered rock fragments (similar δ^7Li to bedrock) (*38*). Both marine authigenic clays and unweathered primary silicate minerals yield higher δ^7Li signatures in siliciclastic sediments relative to continental clays, rendering more negative δ^7Li signatures a reliable indicator for the dominance of continental clays in marine mudstones (*38*, *56*). Complementary evidence comes from the abundance of potassium relative to aluminum (K/Al) in marine mudstones, which also reflects the balance between continental weathering products and marine authigenic clays. The element K is preferentially lost to aqueous solutions relative to Al during chemical weathering of K-bearing primary silicate minerals (e.g., K-feldspar) (*57*), whereas marine clay authigenesis typically involves the incorporation of excess K from seawater or porewater into the clay mineral lattice (*58*). Together, clays derived from continental chemical weathering are expected to record negative δ^7Li and low K/Al values, whereas physically eroded rock fragments and primary silicate minerals tend to exhibit δ^7Li and K/Al values similar to UCC. In contrast, marine authigenic clays are expected to exhibit substantially higher K/Al and δ^7Li values than continentally derived materials, due to uptake of K and isotopically heavy Li from seawater reservoir.

RESULTS

Long-term δ^7Li records presented here for marine mudstones from multiple, geographically disparate regions, spanning the upper Neoproterozoic to middle Cambrian, exhibit a notable shift toward negative values at ~525 Ma (Fig. 1B). Most mudstones deposited before ~525 Ma have δ^7Li values ranging between those of modern UCC (~0 to 1.2‰) and unweathered igneous rocks (~3 to 5‰) (*38*, *54*). Thus, marine mudstones deposited during this period are likely dominated by weakly chemically weathered products, which is consistent with relatively elevated K/Al values recorded in the same suite of samples (Fig. 1A). In addition, relatively higher δ^7Li and K/Al signals before ~525 Ma could also reflect a high relative abundance of marine authigenic clays, particularly in light of extensive marine authigenic clay formation and low seawater δ^7Li values previously inferred for Precambrian oceans (*37*, *50*). By contrast, mudstones deposited after ~525 Ma document negative δ^7Li values (as low as −6‰) and lower K/Al (as low as 0.1), notably lower than those of modern UCC (Fig. 1). Such negative δ^7Li and low K/Al records in marine mudstones are interpreted to reflect relatively high contributions from continentally derived incongruent weathering products (i.e., continental clays),

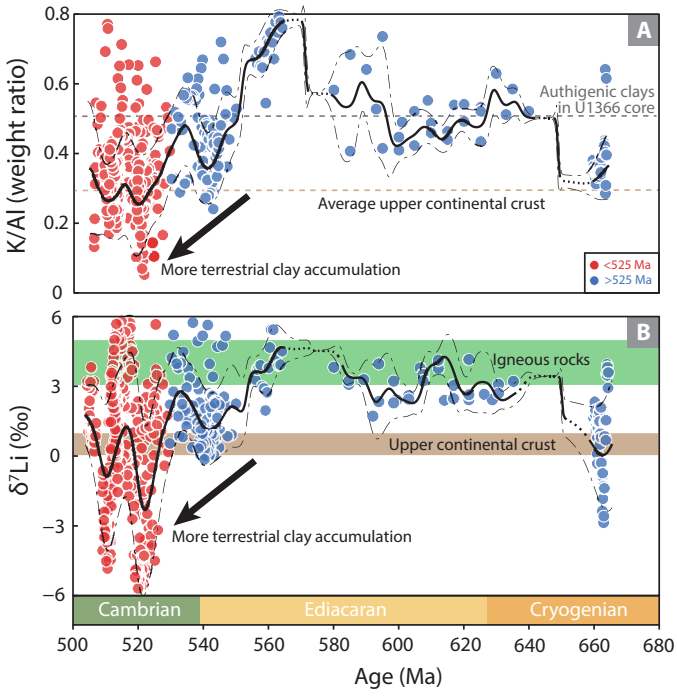

Fig. 1. Marine siliciclastic mudstone δ^7Li and K/Al records from South China, Tarim Bain (northwestern China), Canada, the United States, and Namibia (~660 Ma to 500 Ma). The black curves show weighted smoothing fits for δ^7Li and K/Al data generated in this study with 2 sigma uncertainties (the dotted lines highlight intervals with relatively scarce data). The black and gray dashed lines in (**A**) represent average K/Al ratios of modern UCC (*86*) and authigenic clay–dominated core sediments from the lower part of site U1366 in the South Pacific Gyre (*87*), respectively. The tan and green areas in (**B**) represent the δ^7Li ranges of the modern UCC and igneous rocks, respectively (*54*).

relative to unweathered rock fragments and marine authigenic clays (*55*, *57*, *59*).

DISCUSSION

Shift in Li isotopes of marine mudstones after the early Cambrian

The δ^7Li values of marine mudstones in our dataset exhibit a pronounced inflection in the early Cambrian (~525 Ma), as indicated by both the raw data and the bootstrap-resampled means used to assess the statistical significance of these results (Fig. 2A). Marine mudstones deposited before ~525 Ma exhibit higher δ^7Li values, with the great majority of samples lying between 0 and 3‰. We interpret these samples to reflect predominance by a mixture of poorly weathered rock fragments, potentially with contributions from marine authigenic clays. By contrast, although heavier δ^7Li values also persist, younger mudstones deposited after ~525 are marked by significant shift in distribution to a greater relative abundance of distinctively negative δ^7Li values between −5 and −2‰ (Fig. 2A). Critically, trends in K/Al, to first order, correspond to those described for δ^7Li (Fig. 2B). Therefore, we infer that mudstones deposited before 525 Ma and characterized by both elevated δ^7Li and high K/Al values likely reflect the high relative abundance of poorly weathered continental detrital materials. In addition, following delivery to the continental shelves, the newly formed continental clays may be susceptible to marine authigenesis and exchange with seawater (*37*, *41*, *42*), potentially diluting the preservation of primary continental signals in marine mudstones. Previous studies have proposed that rates of marine clay authigenesis may also have reduced across this interval (*37*, *50*); however, decreases in the extent of marine authigenesis are unlikely to solely cause the notably negative δ^7Li records in mudstones after ~525 Ma without abundant continental clay contribution of isotopically light Li. Together, marine mudstones in our dataset with coupled negative δ^7Li and low K/Al signatures can provide the most conservative estimate of substantial continental clay accumulation in marine sediments. Hence, we interpret samples in our dataset deposited after ~525 Ma to represent pulses of increased continental clay influx to marine sediments.

We further evaluate the characteristics of the analyzed mudstones by examining the relationships between Na/Al, Li/Al, K/Al, and δ^7Li values, based on a modern riverine framework for detrital materials (Fig. 2) (*38*). We normalize elemental abundances to Al concentrations to mitigate possible effects of dilution by quartz and/or organic matter on the geochemical signals recovered. Compared to primary igneous rocks, marine sedimentary rocks are associated with high Li/Al, low Na/Al, and low average δ^7Li values (*38*). Accordingly, a simple mixture of eroded fragments of igneous and sedimentary rocks would result in clear correlations of Na/Al to Li/Al and of δ^7Li to Li/Al between the two endmembers of igneous and sedimentary rocks (Fig. 2, C and D), as seen in modern river sediments (*38*, *60*). However, the absence of clear correlations between endmembers of igneous rock and sedimentary rock observed for the studied mudstones suggests that the lower Cambrian δ^7Li shift observed in our dataset was likely not induced by changes in the provenance (e.g., source lithology) of continental weathering products (Fig. 2, C and D). During chemical weathering of primary silicate minerals, Li, Na, and K are preferentially lost relative to Al (*58*, *59*), leading to lower Li/Al, Na/Al, and K/Al values of continental weathering products relative to crustal precursor lithologies. By contrast, marine reverse weathering would result in additional K and Li accumulation in mudstones, scavenged from seawater or pore water (*48*, *58*). Together, we interpret substantial shifts toward negative δ^7Li and low Na/Al, Li/Al, and K/Al values in marine mudstones, relative to average values of the modern UCC (Fig. 2, B to D), to reflect episodes of enhanced chemical silicate weathering and increased continental clay influx to the continental shelf.

Enhanced continental weathering and clay mineral factory after the early Cambrian

It has been widely argued that, before the proliferation of land plants, continental silicate weathering was predominantly driven by physical erosion during the Precambrian and early Paleozoic, with comparatively limited formation of continental clays (*42*, *61*). Previous research has suggested that marine oxygenation since the Neoproterozoic may have been driven by increased OC burial efficiencies linked to gradual increases in the abundance of phyllosilicates in marine mudstones (*19*), though this framework has subsequently been reinterpreted to reflect enrichments of micaceous minerals (physical eroded products) rather than clays derived from continental chemical weathering (*43*). In this study, mineralogical analyses of typical marine mudstone samples, with either high or low δ^7Li signatures, indicate no substantial changes in aluminosilicate mineralogy from the late Neoproterozoic to the Cambrian. In particular, we do not

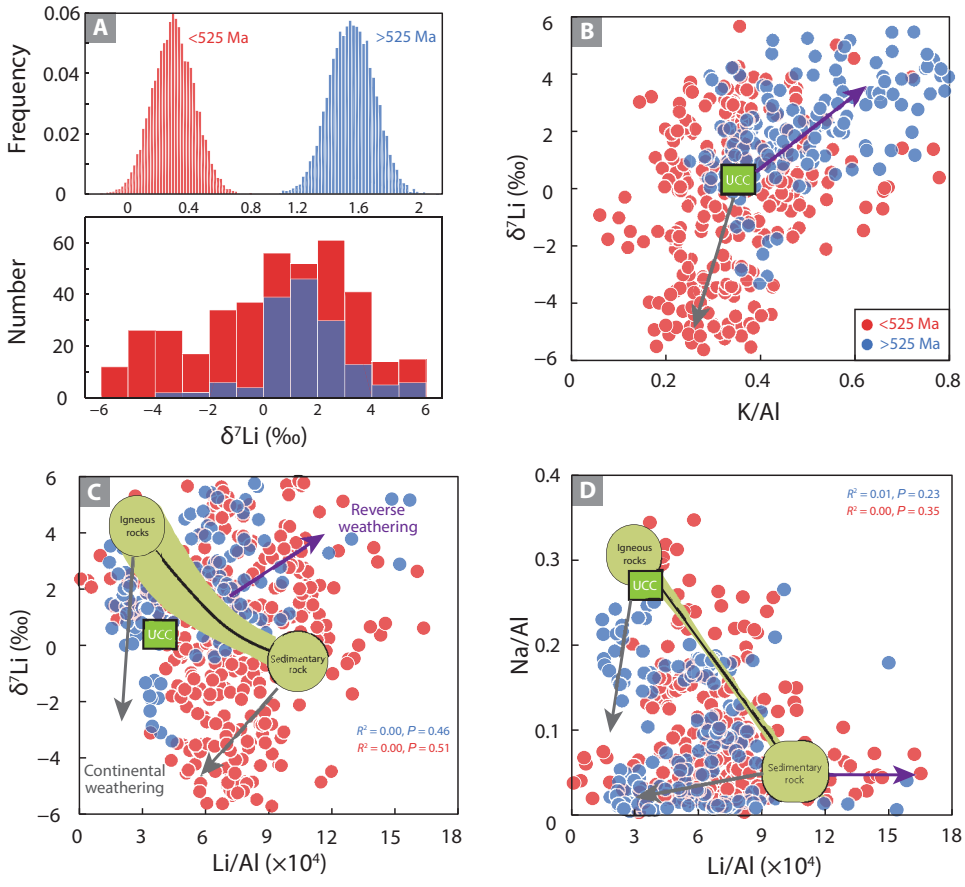

Fig. 2. Analyses of Li isotopes and elemental ratios before and after the early Cambrian (~525 Ma). (**A**) Distribution and bootstrap-resampled means (n = 10,000; generated by repeatedly sampling data from a training dataset and refitting a given model for each sample) for δ^7Li records in marine mudstones deposited before and after the early Cambrian, and cross-plots of (**B**) δ^7Li versus K/Al, (**C**) δ^7Li versus Li/Al, and (**D**) Na/Al versus Li/Al of marine mudstones. The light green areas in (C) and (D) represent "endmember" compositions of igneous rock (Li/Al ≈ 3 parts per million (ppm)/wt %, Na/Al ≈ 0.32, δ^7Li ≈ +4.5‰) and fine-grained sedimentary rock (Li/Al ≈ 9.5 ppm/wt %, Na/Al ≈ 0.08, δ^7Li ≈ −0.5‰) (*38*). The black curve in (C) and line in (D) represent a binary mixture of igneous and sedimentary rock endmembers. The green squares in (B) to (D) represent the average composition of modern UCC (*54*, *86*). The arrows in (B) to (D) denote predicted variations in marine mudstone geochemical composition associated with increases in continental weathering (gray) and marine reverse weathering (purple). Cross-correlation coefficients (R^2) and probability values (P values) were calculated to test the degree of covariations in (C) and (D).

observe notable increases in smectite or kaolinite—clay minerals which are commonly interpreted as products of intense chemical weathering (fig. S2). This lack of an apparent trend in smectite or kaolinite abundance may reflect the postdepositional neomorphism of original clay minerals, highlighting the challenges in identifying long-term patterns in continental weathering and marine authigenesis from clay mineralogy alone (*40*, *41*). In contrast, the geochemical data presented in this study provide independent constraints on the relative abundance of continental clays in marine mudstones. Regardless of uncertainties surrounding original clay mineralogy, coupled negative δ^7Li and low K/Al values provide clear evidence for enrichments in continental clays in marine mudstones after the early Cambrian, linked to shifts in continental chemical weathering regimes and potentially denudation rates. We further attribute increased continental clay formation to the long-term evolution of continental igneous rock composition, global orogeny, and climate warming in the early-middle Cambrian (*62*–*65*). Following the breakup of Rodinia and assembly of Gondwana, the emplacement of large volumes of felsic rock, the development of regionally high continental topography, and increases in CO_2 outgassing rates have been proposed to have occurred in the early Cambrian (*34*, *63*–*65*). The shift in UCC composition during this interval is also reflected by elevated radiogenic Sr isotopes of average continental igneous rocks (*66*) along with decreases in the radiogenic Nd isotope value of marine sediments (*67*). Aligned with global climatic and environmental changes, a shift to more felsic weatherable terranes, characterized by higher Al/(Mg + Ca) ratios, may have preferentially induced more clay formation relative to the products of mafic rock weathering (*68*–*71*). This effect may have been further enhanced by the extreme greenhouse climate (*62*, *63*) and high rates of CO_2 outgassing and orogenesis (*34*, *63*) inferred for the early Cambrian, which may have facilitated the development of floodplains and foreland basins adjacent to mountains, along with a more active hydrological cycle (*72*, *73*). Together, shifts in global tectonic activity and climate during the early Cambrian likely played a critical role in intensifying silicate weathering and continental clay formation before the rise of land plants. Negative δ^7Li signals have also been documented by mudstones deposited during the Cryogenian interglacial interval (Fig. 1B)

and are interpreted to reflect transient increases in silicate weathering intensity due to an increased supply of fresh silicate minerals, a warming climate, and active hydrological conditions during postglacial intervals (*74*). However, this inferred Cryogenian intensification of silicate weathering was ultimately a short-lived response to postglacial perturbation, rather than signaling a secular shift in continental weathering regime (*74*).

Effects of the continental clay mineral factory on global marine redox evolution

Compared to the Neoproterozoic, the early-middle Cambrian may have been marked by an overall decrease in the area of anoxic seafloor although, globally, marine and atmospheric oxygen levels still remained low (*14*, *15*, *75*, *76*). Despite long-standing debates regarding the underlying mechanisms, increased OC burial fluxes were likely the most critical factor in triggering an increase in the baseline of atmospheric and marine oxygen levels between the Proterozoic and the middle Paleozoic (*2*, *8*, *17*). Although subsequent work has questioned whether commonly invoked mechanisms, such as the evolution of complex eukaryotes (*17*), could have feasibly driven a shift in marine export productivity (*21*), other studies have suggested that elevated continental denudation and marine sedimentation rates driven by intensified orogenesis, potentially amplified by increased rates of continental clay influx to continental shelves, could have enhanced OC burial efficiencies and facilitated increases in atmospheric and marine oxygen levels during the early Phanerozoic (*19*, *34*). However, the extent to which changes in continental weathering, nutrient supply, OC burial, and marine redox state are correlated remains poorly constrained. We therefore further compare our Li isotope data to marine mudstone records of phosphorus (P), total OC (TOC), and uranium (U) contents from the Sedimentary Geochemistry and Paleoenvironments Project (SGP) database (*77*). Assessment of SGP compilations, drawing on more than 6000 independent sedimentary records, allows us to approximate global-scale patterns in average nutrient availability, OC burial, and marine oxygenation from the late Neoproterozoic to the Cambrian (Fig. 3, B to D) (*12*). Although we have not analyzed these data in a multivariate framework or accounted for sampling biases, the first-order pattern shows systematic increases in the TOC and U contents of marine mudstones across this interval, suggesting that enhanced OC burial in marine sediments and decreased global anoxic seafloor area (*12*, *16*, *18*, *78*, *79*) appear to be coincident with shifts in δ^7Li toward more negative values (Fig. 3). The transition of primary-producer communities from predominantly cyanobacteria to eukaryotic algae and increased seawater nutrient (e.g., P) levels have been proposed to have enhanced marine productivity and fostered a more efficient biological pump since the Neoproterozoic. However, the initial rise of eukaryotic algae and marine P availability occurred in the early Neoproterozoic (*8*, *20*), substantially earlier than the increase in TOC and U contents in the SGP compilations (Fig. 3). On the basis of comparisons of our newly analyzed and compiled sedimentary δ^7Li, TOC, U, and P data, we suggest that intensified OC burial across this interval may instead have been primarily controlled by increased influx of continental clay to marine sediments in continental shelf settings (Fig. 3). New P compilations in this study also show appreciable peaks after ~525 Ma (Fig. 3B), potentially indicative of an increased marine P reservoir. In addition to possible post-Ediacaran reorganization of the marine P cycle (*80*), enhanced continental weathering, as identified by sedimentary δ^7Li records in this study, as well as increases in average crustal P concentrations (*81*), could have contributed to elevated marine P availability in the early Cambrian.

Building on our geochemical data, we further used a global biogeochemical multiple-box model (*33*) to evaluate the effects of enhanced silicate weathering and continental clay formation on global carbon, oxygen, and nutrient cycling, with additional parameterization to represent the protection of OC by continental clay minerals (see the Supplementary Materials for detailed model description). The initial continental clay influx to continental shelf sediments was assumed to be 25% of modern values, a value selected to represent low chemical weathering intensity and limited continental clay formation during the Proterozoic (*19*, *42*). We then simulated shifts in atmospheric pO_2, dissolved O_2 concentration in the deep ocean, and the efficiency of OC burial on the continental shelf accompanied by gradual increases in continental clay influx to continental shelf sediments (Fig. 4). The terrestrial OC burial flux was set to zero in these simulations with the assumption of extremely limited terrestrial export productivity before the rise of land plants. Given estimated pO_2 levels of 5 to 40% PAL (present atmospheric level) for the late Neoproterozoic atmosphere (*82*), our model results suggest that gradually accelerated continental clay delivery to continental shelves could lead to notable increases in OC burial efficiency. This shift in OC burial efficiency, in turn, could have led to relatively substantial (albeit still low in absolute magnitude, compared to the modern Earth system) increases in atmospheric and marine oxygen levels. For instance, a twofold increase in the burial flux of continental clays in marine sediments following the early Cambrian, as also estimated in (*19*), could have resulted in a ~50% increase in atmospheric pO_2 and an approximately eightfold increase in the dissolved O_2 concentrations of the intermediate-depth and deep ocean (>100-m depth in the model) (Fig. 4). Future work will hopefully further resolve remaining uncertainties regarding the scope of clay-OC interactions. However, these data indicate that changes in continental clay formation and delivery can potentially serve as important levers on the global oxygen cycle. In sum, the synthesis of our Li isotope data and the results of this numerical modeling exercise indicate that amplified delivery of continental clays to coastal and shallow-marine settings may have facilitated increases in atmospheric and global ocean levels after the early Cambrian (*14*, *15*, *75*, *82*). Although early Paleozoic oxygen levels were likely characterized by lower and more variable oxygen levels than those of the modern Earth (Fig. 3) (*13*, *14*, *16*, *82*), increases in continental clay production and delivery may have decreased sedimentary dissolved oxygen consumption, leading to a progressive expansion of oxygenated seawater during the early radiation of animals.

MATERIALS AND METHODS

Sampling

In this study, the Li isotope and K/Al data are largely based on classic stratotype sections with well-established biostratigraphic, chemostratigraphic, and chronostratigraphic frameworks. The sampling intervals are illustrated in fig. S1, mainly consisting of mudstones, shales, and silty shales from the following: (i) South China: Cryogenian Datangpo Formation; Ediacaran Doushantuo Formation (Member II and Miaohe Member) and Lantian Formation (Member II); lower Cambrian Liuchapo Formation, Yanjiahe Formation, Shuijingtuo Formation, Jiumenchong Formation, Niutitang Formation, and Zhalagou Formation; middle Cambrian Shipa Formation, Balang Formation, Duliujiang Formation, and Kaili Formation. (ii) Canada:

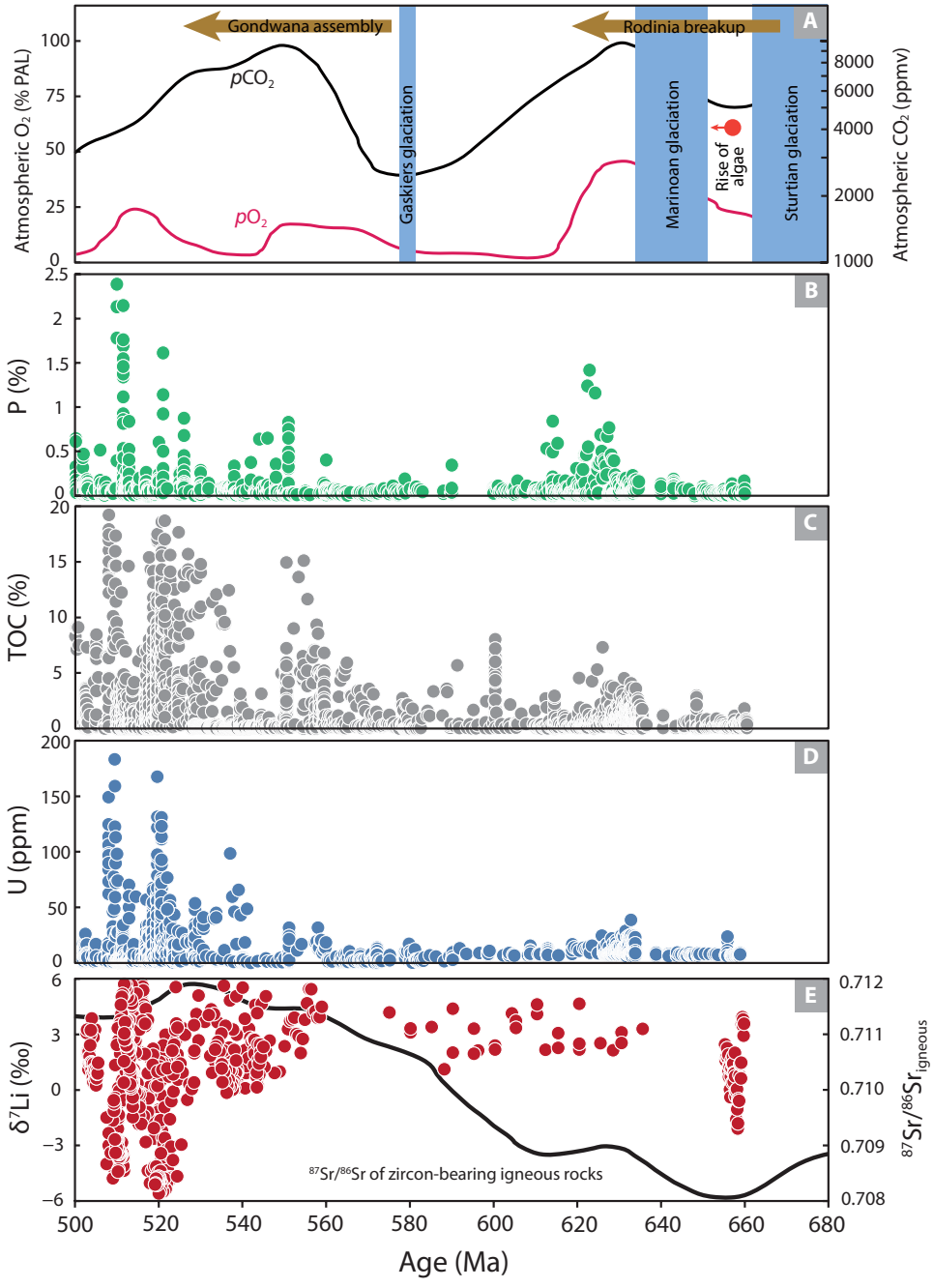

Fig. 3. Long-term records of δ^7Li, U content, TOC content, and P content in marine mudstones, and key environmental evolution from the Cryogenian to the middle Cambrian (~660 Ma to 500 Ma). (**A**) The key biotic, environmental, and tectonic events (*8*, *12*) and curves of atmospheric CO_2 (in parts per million by volume) and atmospheric O_2 relative to present atmospheric level (PAL) from the NEOCARBSULF model (*82*). Data compilations of (**B**) P content, (**C**) TOC content, and (**D**) U contents are from Sedimentary Geochemistry and Paleoenvironments Project (*77*); (**E**) δ^7Li data generated by this study, and evolution of average $^{87}Sr/^{86}Sr$ ratios of zircon-bearing igneous rocks (black curve) (*66*).

lower Cambrian Ingta Formation, Mural Formation, and Mahto Formation; middle Cambrian Burgess Shale. (iii) United States: lower Cambrian Parker Slate, middle Cambrian Pioche Formation, Wheeler Formation, Marjum Formation, and Langston Formation. (iv) Namibia: uppermost Ediacaran to lowermost Cambrian Spitskopf Formation (Feldschuhhorn Member) and Nomtsas Formation. (v) Tarim basin, North China: lower Cambrian Yuertusi Formation. Detailed information for sample sites, ages, and stratigraphic correlations is presented in section S1 of the Supplementary Materials.

Elemental and isotopic analyses

For trace element and isotope analyses, sample powders were first rinsed using 1 M acetic acid to remove carbonate components from bulk mudstones. The residuals were fully digested with distilled acids

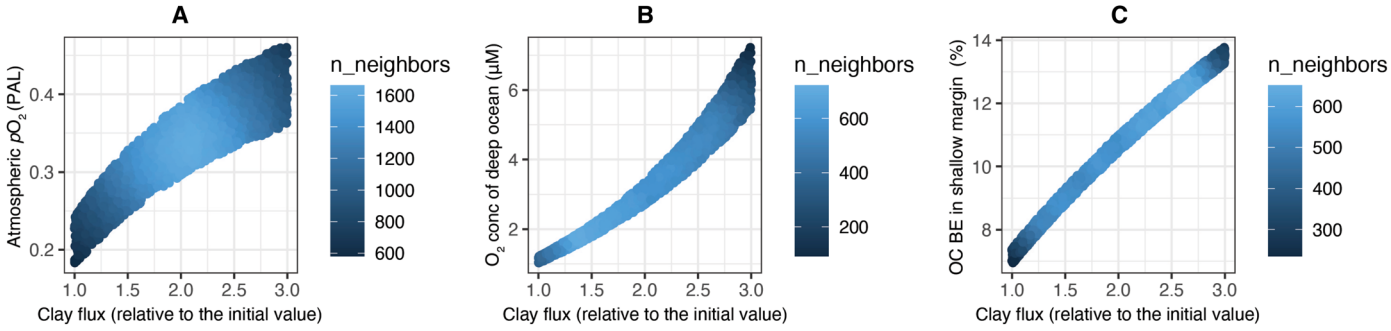

Fig. 4. Monte Carlo model results for the influence of continental clay burial in marine settings on marine organic carbon burial and redox evolution. (**A**) Changes in atmospheric O_2 (PAL, present atmospheric level). (**B**) Changes in dissolved O_2 in the deep ocean (in micromolar). (**C**) Changes in OC burial efficiency (BE). The initial continental clay flux was set to be 25% of that of modern levels. The Monte Carlo simulation was performed by randomly sampling the continental clay burial flux (25 to 75% of the present level) and the continental phosphorus weathering flux (50 to 60% of the present level). The Monte Carlo simulation was run 7000 times. The parameter n_neighbors refers to the number of neighboring points considered when estimating the density of points in a scatterplot (see the Supplementary Materials for further discussion of this simulation).

of HF, HNO_3, and HCl. Major and trace elements of the samples were analyzed with a Thermo Scientific Element XR ICP-MS (Inductively Coupled Plasma Mass Spectrometer) at the Yale Metal Geochemistry Center (YMGC), Yale University, and the Metal Isotope Geochemistry Lab in the Centre for Research and Education on Biological Evolution and Environment (CREBEE), Nanjing University. Lithium isotopes were analyzed with a Thermo Scientific Neptune Plus/XT MC-ICP-MS (Multicollector-Inductively Coupled Plasma Mass Spectrometer) combined with an ESI Apex-IR desolvating system at YMGC and CREBEE. Each sample, containing 50 ng of Li, was purified using AG50W-X12 (200 to 400 mesh) cation resin with 0.2 M HCl. Detailed descriptions of sample preparation, analytical methods, and accuracy follow that of previous studies (*74*) and are presented in the Supplementary Materials.

The global biogeochemical model

Our biogeochemical model is modified from a six-box global biogeochemical model, which includes representation of the carbon, oxygen, sulfur, iron, and phosphorus cycles (*33*). The main modification from the previous model is that we have linked OC burial efficiencies not only to iron minerals but also to clay burial fluxes. We have assumed a fixed fraction of OC burial associated with Fe oxides (OC/Fe ratio of 4), following previous studies (*33*, *83*). The initial clay sedimentation flux was set to be 25% of that of modern continental shelf settings (*19*, *84*), to reflect low continental clay fluxes to marine sediments during the Proterozoic. Terrestrial export productivity was set to 0 in these simulations, under the assumption that limited OC burial occurred on land before the rise of land plants. Initial atmospheric O_2 levels were set at 5 to 40% PAL, based on previous estimates generated by well-established numerical models (*82*, *85*). Detailed descriptions of the model parameters and sensitivity tests are presented in the Supplementary Materials.

Supplementary Materials

This PDF file includes:
Supplementary text S1 to S3
Figs. S1 to S5
Legends for data S1 and S2
References

Other Supplementary Material for this manuscript includes the following:
Data S1 and S2

REFERENCES AND NOTES

1. L. R. Kump, The rise of atmospheric oxygen. *Nature* **451**, 277–278 (2008).
2. C.-T. A. Lee, L. Y. Yeung, N. R. McKenzie, Y. Yokoyama, K. Ozaki, A. Lenardic, Two-step rise of atmospheric oxygen linked to the growth of continents. *Nat. Geosci.* **9**, 417–424 (2016).
3. C. T. Reinhard, N. J. Planavsky, Biogeochemical controls on the redox evolution of Earth's oceans and atmosphere. *Elements* **16**, 191–196 (2020).
4. T. W. Lyons, C. T. Reinhard, N. J. Planavsky, The rise of oxygen in Earth's early ocean and atmosphere. *Nature* **506**, 307–315 (2014).
5. A. H. Knoll, M. A. Nowak, The timetable of evolution. *Sci. Adv.* **3**, e1603076 (2017).
6. R. A. Berner, Modeling atmospheric O2 over Phanerozoic time. *Geochim. Cosmochim. Acta* **65**, 685–694 (2001).
7. L. J. Alcott, B. J. W. Mills, S. W. Poulton, Stepwise Earth oxygenation is an inherent property of global biogeochemical cycling. *Science* **366**, 1333–1337 (2019).
8. J. J. Brocks, A. J. M. Jarrett, E. Sirantoine, C. Hallmann, Y. Hoshino, T. Liyanage, The rise of algae in Cryogenian oceans and the emergence of animals. *Nature* **548**, 578–581 (2017).
9. M. Zhao, S. Zhang, L. G. Tarhan, C. T. Reinhard, N. Planavsky, The role of calcium in regulating marine phosphorus burial and atmospheric oxygenation. *Nat. Commun.* **11**, 2232 (2020).
10. J. P. Dunne, J. L. Sarmiento, A. Gnanadesikan, A synthesis of global particle export from the surface ocean and cycling through the ocean interior and on the seafloor. *Global Biogeochem. Cycles* **21**, 2006GB002907 (2007).
11. D. J. Burdige, Preservation of organic matter in marine sediments: Controls, mechanisms, and an imbalance in sediment organic carbon budgets? *Chem. Rev.* **107**, 467–485 (2007).
12. L. M. Och, G. A. Shields-Zhou, The Neoproterozoic oxygenation event: Environmental perturbations and biogeochemical cycling. *Earth-Sci. Rev.* **110**, 26–57 (2012).
13. E. A. Sperling, C. J. Wolock, A. S. Morgan, B. C. Gill, M. Kunzmann, G. P. Halverson, F. A. Macdonald, A. H. Knoll, D. T. Johnston, Statistical analysis of iron geochemical data suggests limited late Proterozoic oxygenation. *Nature* **523**, 451–454 (2015).
14. D. A. Stolper, C. B. Keller, A record of deep-ocean dissolved O_2 from the oxidation state of iron in submarine basalts. *Nature* **553**, 323–327 (2018).
15. G.-Y. Wei, H.-F. Ling, G. A. Shields, S. V. Hohl, T. Yang, Y.-B. Lin, F. Zhang, Revisiting stepwise ocean oxygenation with authigenic barium enrichments in marine mudrocks. *Geology* **49**, 1059–1063 (2021).
16. G.-Y. Wei, N. J. Planavsky, T. He, F. Zhang, R. Stockey, D. B. Cole, Y.-B. Lin, H.-F. Ling, Global marine redox evolution from the late Neoproterozoic to the early Paleozoic constrained by the integration of Mo and U isotope records. *Earth-Sci. Rev.* **214**, 103506 (2021).
17. T. M. Lenton, R. A. Boyle, S. W. Poulton, G. A. Shields-Zhou, N. J. Butterfield, Co-evolution of eukaryotes and ocean oxygenation in the Neoproterozoic era. *Nat. Geosci.* **7**, 257–265 (2014).
18. E. A. Sperling, R. G. Stockey, The temporal and environmental context of early animal evolution: Considering all the ingredients of an "Explosion". *Integr. Comp. Biol.* **58**, 605–622 (2018).
19. M. Kennedy, M. Droser, L. Mayer, D. Pevear, D. Mrofka, Late Precambrian oxygenation; inception of the clay mineral factory. *Science* **311**, 1446–1449 (2006).

20. N. J. Planavsky, D. Asael, A. D. Rooney, L. J. Robbins, B. C. Gill, C. M. Dehler, D. B. Cole, S. M. Porter, G. D. Love, K. O. Konhauser, C. T. Reinhard, A sedimentary record of the evolution of the global marine phosphorus cycle. *Geobiology* **21**, 168–174 (2023).
21. M. Fakhraee, N. J. Planavsky, C. T. Reinhard, The role of environmental factors in the long-term evolution of the marine biological pump. *Nat. Geosci.* **13**, 812–816 (2020).
22. J. I. Hedges, R. G. Keil, Sedimentary organic matter preservation: An assessment and speculative synthesis. *Mar. Chem.* **49**, 81–115 (1995).
23. S. Arndt, B. B. Jørgensen, D. E. LaRowe, J. J. Middelburg, R. D. Pancost, P. Regnier, Quantifying the degradation of organic matter in marine sediments: A review and synthesis. *Earth-Sci. Rev.* **123**, 53–86 (2013).
24. D. E. LaRowe, S. Arndt, J. A. Bradley, E. R. Estes, A. Hoarfrost, S. Q. Lang, K. G. Lloyd, N. Mahmoudi, W. D. Orsi, S. R. Shah Walter, A. D. Steen, R. Zhao, The fate of organic carbon in marine sediments - New insights from recent data and analysis. *Earth-Sci. Rev.* **204**, 103146 (2020).
25. E. J. W. Wattel- Koekkoek, P. Buurman, J. Van Der Plicht, E. Wattel, N. Van Breemen, Mean residence time of soil organic matter associated with kaolinite and smectite. *Eur. J. Soil Sci.* **54**, 269–278 (2003).
26. T. S. Arnarson, R. G. Keil, Changes in organic matter–mineral interactions for marine sediments with varying oxygen exposure times. *Geochim. Cosmochim. Acta* **71**, 3545–3556 (2007).
27. J. D. Hemingway, D. H. Rothman, K. E. Grant, S. Z. Rosengard, T. I. Eglinton, L. A. Derry, V. V. Galy, Mineral protection regulates long-term global preservation of natural organic carbon. *Nature* **570**, 228–231 (2019).
28. K.-Q. Xiao, Y. Zhao, C. Liang, M. Zhao, O. W. Moore, A. Otero-Fariña, Y.-G. Zhu, K. Johnson, C. L. Peacock, Introducing the soil mineral carbon pump. *Nat. Rev. Earth Environ.* **4**, 135–136 (2023).
29. B. Ransom, D. Kim, M. Kastner, S. Wainwright, Organic matter preservation on continental slopes: Importance of mineralogy and surface area. *Geochim. Cosmochim. Acta* **62**, 1329–1345 (1998).
30. M. J. Kennedy, T. Wagner, Clay mineral continental amplifier for marine carbon sequestration in a greenhouse ocean. *Proc. Natl. Acad. Sci. U.S.A.* **108**, 9776–9781 (2011).
31. T. M. Blattmann, Z. Liu, Y. Zhang, Y. Zhao, N. Haghipour, D. B. Montlucon, M. Plotze, T. I. Eglinton, Mineralogical control on the fate of continentally derived organic matter in the ocean. *Science* **366**, 742–745 (2019).
32. H. Shang, D. H. Rothman, G. P. Fournier, Oxidative metabolisms catalyzed Earth's oxygenation. *Nat. Commun.* **13**, 1328 (2022).
33. M. Y. Zhao, B. J. W. Mills, W. B. Homoky, C. L. Peacock, Oxygenation of the Earth aided by mineral-organic carbon preservation. *Nat. Geosci.* **16**, 262–267 (2023).
34. I. H. Campbell, R. J. Squire, The mountains that triggered the late neoproterozoic increase in oxygen: The second great oxidation event. *Geochim. Cosmochim. Acta* **74**, 4187–4206 (2010).
35. A. C. Aplin, J. H. S. Macquaker, Mudstone diversity: Origin and implications for source, seal, and reservoir properties in petroleum systems. *AAPG Bulletin* **95**, 2031–2059 (2011).
36. F. T. Mackenzie, L. R. Kump, Reverse weathering, clay mineral formation, and oceanic element cycles. *Science* **270**, 586 (1995).
37. T. T. Isson, N. J. Planavsky, Reverse weathering as a long-term stabilizer of marine pH and planetary climate. *Nature* **560**, 471–475 (2018).
38. M. Dellinger, J. Gaillardet, J. Bouchez, D. Calmels, V. Galy, R. G. Hilton, P. Louvat, C. France-Lanord, Lithium isotopes in large rivers reveal the cannibalistic nature of modern continental weathering and erosion. *Earth Planet. Sci. Lett.* **401**, 359–372 (2014).
39. G. Steinhoefel, S. L. Brantley, M. S. Fantle, Lithium isotopic fractionation during weathering and erosion of shale. *Geochim. Cosmochim. Acta* **295**, 155–177 (2021).
40. G. D. De Segonzac, The transformation of clay minerals during diagenesis and low-grade metamorphism: A review. *Sedimentology* **15**, 281–346 (1970).
41. J. Kim, H. Dong, J. Seabaugh, S. W. Newell, D. D. Eberl, Role of microbes in the smectite-to-illite reaction. *Science* **303**, 830–832 (2004).
42. M. Rafiei, M. Kennedy, Weathering in a world without terrestrial life recorded in the Mesoproterozoic Velkerri Formation. *Nat. Commun.* **10**, 3448 (2019).
43. N. J. Tosca, D. T. Johnston, A. Mushegian, D. H. Rothman, R. E. Summons, A. H. Knoll, Clay mineralogy, organic carbon burial, and redox evolution in Proterozoic oceans. *Geochim. Cosmochim. Acta* **74**, 1579–1592 (2010).
44. R. L. Rudnick, P. B. Tomascak, H. B. Njo, L. R. Gardner, Extreme lithium isotopic fractionation during continental weathering revealed in saprolites from South Carolina. *Chem. Geol.* **212**, 45–57 (2004).
45. N. Vigier, A. Decarreau, R. Millot, J. Carignan, S. Petit, C. France-Lanord, Quantifying Li isotope fractionation during smectite formation and implications for the Li cycle. *Geochim. Cosmochim. Acta* **72**, 780–792 (2008).
46. J. Wimpenny, S. R. Gíslason, R. H. James, A. Gannoun, P. A. E. Pogge Von Strandmann, K. W. Burton, The behaviour of Li and Mg isotopes during primary phase dissolution and secondary mineral formation in basalt. *Geochim. Cosmochim. Acta* **74**, 5259–5279 (2010).
47. W. Li, X.-M. Liu, Experimental investigation of lithium isotope fractionation during kaolinite adsorption: Implications for chemical weathering. *Geochim. Cosmochim. Acta* **284**, 156–172 (2020).
48. C.-Y. Liu, D. J. Wilson, E. C. Hathorne, A. Xu, P. A. E. Pogge von Strandmann, The influence of river-derived particles on estuarine and marine elemental cycles: Evidence from lithium isotopes. *Geochim. Cosmochim. Acta* **361**, 183–199 (2023).
49. E. Andrews, P. A. E. Pogge von Strandmann, M. S. Fantle, Exploring the importance of authigenic clay formation in the global Li cycle. *Geochim. Cosmochim. Acta* **289**, 47–68 (2020).
50. B. Kalderon-Asael, J. A. R. Katchinoff, N. J. Planavsky, A. V. S. Hood, M. Dellinger, E. J. Bellefroid, D. S. Jones, A. Hofmann, F. O. Ossa, F. A. Macdonald, C. Wang, T. T. Isson, J. G. Murphy, J. A. Higgins, A. J. West, M. W. Wallace, D. Asael, P. A. E. P. von Strandmann, A lithium-isotope perspective on the evolution of carbon and silicon cycles. *Nature* **595**, 394–398 (2021).
51. L.-H. Chan, J. C. Alt, D. A. H. Teagle, Lithium and lithium isotope profiles through the upper oceanic crust: A study of seawater–basalt exchange at ODP Sites 504B and 896A. *Earth Planet. Sci. Lett.* **201**, 187–201 (2002).
52. L.-H. Chan, W. P. Leeman, T. Plank, Lithium isotopic composition of marine sediments. *Geochem. Geophys. Geosyst.* **7**, Q06005 (2006).
53. S. Misra, P. N. Froelich, Lithium isotope history of cenozoic seawater: Changes in silicate weathering and reverse weathering. *Science* **335**, 818–823 (2012).
54. L. Sauzéat, R. L. Rudnick, C. Chauvel, M. Garçon, M. Tang, New perspectives on the Li isotopic composition of the upper continental crust and its weathering signature. *Earth Planet. Sci. Lett.* **428**, 181–192 (2015).
55. M. Dellinger, J. Bouchez, J. Gaillardet, L. Faure, J. Moureau, Tracing weathering regimes using the lithium isotope composition of detrital sediments. *Geology* **45**, 411–414 (2017).
56. W. Wei, T. J. Algeo, Secular variation in the elemental composition of marine shales since 840 Ma: Tectonic and seawater influences. *Geochim. Cosmochim. Acta* **287**, 367–390 (2020).
57. G. Bayon, I. N. Bindeman, A. Trinquier, G. J. Retallack, A. Bekker, Long-term evolution of terrestrial weathering and its link to Earth's oxygenation. *Earth Planet. Sci. Lett.* **584**, 117490 (2022).
58. C. M. Fedo, H. Wayne Nesbitt, G. M. Young, Unraveling the effects of potassium metasomatism in sedimentary rocks and paleosols, with implications for paleoweathering conditions and provenance. *Geology* **23**, 921–924 (1995).
59. H. W. Nesbitt, G. Markovics, R. C. Price, Chemical processes affecting alkalis and alkaline earths during continental weathering. *Geochim. Cosmochim. Acta.* **44**, 1659–1666 (1980).
60. C. Yang, N. Vigier, S. Yang, M. Revel, L. Bi, Clay Li and Nd isotopes response to hydroclimate changes in the Changjiang (Yangtze) basin over the past 14,000 years. *Earth Planet. Sci. Lett.* **561**, 116793 (2021).
61. W. J. McMahon, N. S. Davies, Evolution of alluvial mudrock forced by early land plants. *Science* **359**, 1022–1024 (2018).
62. T. W. Hearing, T. H. P. Harvey, M. Williams, M. J. Leng, A. L. Lamb, P. R. Wilby, S. E. Gabbott, A. Pohl, Y. Donnadieu, An early Cambrian greenhouse climate. *Sci. Adv.* **4**, eaar5690 (2018).
63. N. R. McKenzie, B. K. Horton, S. E. Loomis, D. F. Stockli, N. J. Planavsky, C.-T. A. Lee, Continental arc volcanism as the principal driver of icehouse-greenhouse variability. *Science* **352**, 444–447 (2016).
64. Z.-X. Li, D. A. D. Evans, G. P. Halverson, Neoproterozoic glaciations in a revised global palaeogeography from the breakup of Rodinia to the assembly of Gondwanaland. *Sediment. Geol.* **294**, 219–232 (2013).
65. T. R. Worsley, D. Nance, J. B. Moody, Global tectonics and eustasy for the past 2 billion years. *Mar. Geol.* **58**, 373–400 (1984).
66. C. P. Bataille, A. Willis, X. Yang, X. M. Liu, Continental igneous rock composition: A major control of past global chemical weathering. *Sci. Adv.* **3**, e1602183 (2017).
67. G.-Y. Wei, H.-F. Ling, G. A. Shields, T. Chen, M. Lechte, X. Chen, C. Qiu, H. Lei, M. Zhu, Long-term evolution of terrestrial inputs from the Ediacaran to early Cambrian: Clues from Nd isotopes in shallow-marine carbonates, South China. *Palaeogeogr. Palaeoclimatol. Palaeoecol.* **535**, 109367 (2019).
68. Y. Tardy, G. Bocquier, H. Paquet, G. Millot, Formation of clay from granite and its distribution in relation to climate and topography. *Geoderma* **10**, 271–284 (1973).
69. P. Amiotte Suchet, J.-L. Probst, W. Ludwig, Worldwide distribution of continental rock lithology: Implications for the atmospheric/soil CO_2 uptake by continental weathering and alkalinity river transport to the oceans. *Global Biogeochem. Cycles* **17**, 1038 (2003).
70. J. Hartmann, A. J. West, P. Renforth, P. Köhler, C. L. De La Rocha, D. A. Wolf-Gladrow, H. H. Dürr, J. Scheffran, Enhanced chemical weathering as a geoengineering strategy to reduce atmospheric carbon dioxide, supply nutrients, and mitigate ocean acidification. *Rev. Geophys.* **51**, 113–149 (2013).
71. R. M. Hazen, D. A. Sverjensky, D. Azzolini, D. L. Bish, S. C. Elmore, L. Hinnov, R. E. Milliken, Clay mineral evolution. *Am. Mineral.* **98**, 2007–2029 (2013).
72. C. Hoorn, F. P. Wesselingh, H. ter Steege, M. A. Bermudez, A. Mora, J. Sevink, I. Sanmartín, A. Sanchez-Meseguer, C. L. Anderson, J. P. Figueiredo, C. Jaramillo, D. Riff, F. R. Negri, H. Hooghiemstra, J. Lundberg, T. Stadler, T. Särkinen, A. Antonelli, Amazonia through time: Andean uplift, climate change, landscape evolution, and biodiversity. *Science* **330**, 927–931 (2010).

73. A. Ielpi, P. Fralick, D. Ventra, M. Ghinassi, L. E. Lebeau, A. Marconato, R. Meek, R. H. Rainbird, Fluvial floodplains prior to greening of the continents: Stratigraphic record, geodynamic setting, and modern analogues. *Sediment. Geol.* **372**, 140–172 (2018).
74. G.-Y. Wei, W. Wei, D. Wang, T. Li, X. Yang, G. A. Shields, F. Zhang, G. Li, T. Chen, T. Yang, H.-F. Ling, Enhanced chemical weathering triggered an expansion of euxinic seawater in the aftermath of the Sturtian glaciation. *Earth Planet. Sci. Lett.* **539**, 116244 (2020).
75. C. Li, C. Jin, N. J. Planavsky, T. J. Algeo, M. Cheng, X. Yang, Y. Zhao, S. Xie, Coupled oceanic oxygenation and metazoan diversification during the early–middle Cambrian? *Geology* **45**, 743–746 (2017).
76. L. Jiang, M. Zhao, A. Shen, L. Huang, D. Chen, C. Cai, Pulses of atmosphere oxygenation during the Cambrian radiation of animals. *Earth Planet. Sci. Lett.* **590**, 117565 (2022).
77. Ú. C. Farrell, R. Samawi, S. Anjanappa, R. Klykov, O. O. Adeboye, H. Agic, A.-S. C. Ahm, T. H. Boag, F. Bowyer, J. J. Brocks, T. N. Brunoir, D. E. Canfield, X. Chen, M. Cheng, M. O. Clarkson, D. B. Cole, D. R. Cordie, P. W. Crockford, H. Cui, T. W. Dahl, L. D. Mouro, K. Dewing, S. Q. Dornbos, N. Drabon, J. A. Dumoulin, J. F. Emmings, C. R. Endriga, T. A. Fraser, R. R. Gaines, R. M. Gaschnig, T. M. Gibson, G. J. Gilleaudeau, B. C. Gill, K. Goldberg, R. Guilbaud, G. P. Halverson, E. U. Hammarlund, K. G. Hantsoo, M. A. Henderson, M. S. W. Hodgskiss, T. J. Horner, J. M. Husson, B. Johnson, P. Kabanov, C. B. Keller, J. Kimmig, M. A. Kipp, A. H. Knoll, T. Kreitsmann, M. Kunzmann, F. Kurzweil, M. A. Le Roy, C. Li, A. G. Lipp, D. K. Loydell, X. Lu, F. A. Macdonald, J. M. Magnall, K. Mänd, A. Mehra, M. J. Melchin, A. J. Miller, N. T. Mills, C. N. Mwinde, B. O'Cennell, L. M. Och, F. O. Ossa, A. Pagès, K. Paiste, C. A. Partin, S. E. Peters, P. Petrov, T. L. Playter, S. Plaza-Torres, S. M. Porter, S. W. Poulton, S. B. Pruss, S. Richoz, S. R. Ritzer, A. D. Rooney, S. K. Sahoo, S. D. Schoepfer, J. A. Sclafani, Y. Shen, O. Shorttle, S. P. Slotznick, E. F. Smith, S. Spinks, R. G. Stockey, J. V. Strauss, E. E. Stüeken, S. Tecklenburg, D. Thomson, N. J. Tosca, G. J. Uhlein, M. N. Vizcaíno, H. Wang, T. White, P. R. Wilby, C. R. Woltz, R. A. Wood, L. Xiang, I. A. Yurchenko, T. Zhang, N. J. Planavsky, K. V. Lau, D. T. Johnston, E. A. Sperling, The sedimentary geochemistry and paleoenvironments project. *Geobiology* **19**, 545–556 (2021).
78. C. A. Partin, A. Bekker, N. J. Planavsky, C. T. Scott, B. C. Gill, C. Li, V. Podkovyrov, A. Maslov, K. O. Konhauser, S. V. Lalonde, G. D. Love, S. W. Poulton, T. W. Lyons, Large-scale fluctuations in Precambrian atmospheric and oceanic oxygen levels from the record of U in shales. *Earth Planet. Sci. Lett.* **369-370**, 284–293 (2013).
79. M. Cheng, C. Li, C. Jin, H. Wang, T. J. Algeo, T. W. Lyons, F. Zhang, A. Anbar, Evidence for high organic carbon export to the early Cambrian seafloor. *Geochim. Cosmochim. Acta* **287**, 125–140 (2020).
80. T. A. Laakso, E. A. Sperling, D. T. Johnston, A. H. Knoll, Ediacaran reorganization of the marine phosphorus cycle. *Proc. Natl. Acad. Sci. U.S.A.* **117**, 11961–11967 (2020).
81. C. R. Walton, J. Hao, F. Huang, F. E. Jenner, H. Williams, A. L. Zerkle, A. Lipp, R. M. Hazen, S. E. Peters, O. Shorttle, Evolution of the crustal phosphorus reservoir. *Sci. Adv.* **9**, eade6923 (2023).
82. A. J. Krause, B. J. W. Mills, A. S. Merdith, T. M. Lenton, S. W. Poulton, Extreme variability in atmospheric oxygen levels in the late Precambrian. *Sci. Adv.* **8**, eabm8191 (2022).
83. K. Lalonde, A. Mucci, A. Ouellet, Y. Gelinas, Preservation of organic matter in sediments promoted by iron. *Nature* **483**, 198–200 (2012).
84. J. J. Griffin, H. Windom, E. D. Goldberg, The distribution of clay minerals in the World Ocean. *Deep-Sea Res. Oceanogr. Abstr.* **15**, 433–459 (1968).
85. T. M. Lenton, S. J. Daines, B. J. W. Mills, COPSE reloaded: An improved model of biogeochemical cycling over Phanerozoic time. *Earth-Sci. Rev.* **178**, 1–28 (2018).
86. R. L. Rudnick, S. Gao, The composition of the continental crust, in *Treatise on Geochemistry*, vol. 3, *The Crust*, H. D. Holland, K. K. Turekian, Eds. (Elsevier-Pergamon, 2014), pp. 1–64.
87. A. G. Dunlea, R. W. Murray, J. Sauvage, A. J. Spivack, R. N. Harris, S. D'Hondt, Dust, volcanic ash, and the evolution of the South Pacific Gyre through the Cenozoic. *Paleoceanography* **30**, 1078–1099 (2015).
88. G. S. Nowlan, G. M. Narbonne, W. H. Fritz, Small shelly fossils and trace fossils near the Precambrian-Cambrian boundary in the Yukon Territory, Canada. *Lethaia* **18**, 233–256 (1985).
89. L. J. Pyle, G. M. Narbonne, G. S. Nowlan, S. Xiao, N. P. James, Early cambrian metazoan eggs, embryos, and phosphatic microfossils from northwestern canada. *J. Paleo.* **80**, 811–825 (2006).
90. J. D. Aitken, Uppermost proterozoic formations in central mackenzie mountains, northwest territories. *Bull. Geol. Surv. Canada* **368**, 1–24 (1989).
91. C. Carbone, G. M. Narbonne, When life got smart: The evolution of behavioral complexity through the Ediacaran and early Cambrian of NW Canada. *J. Paleo.* **88**, 309–330 (2014).
92. W. H. Fritz, E. W. Mountjoy, Lower and early Middle Cambrian formations near Mount Robson, British Columbia and Alberta. *Can. J. Earth Sci.* **12**, 119–131 (1975).
93. E. A. Sperling, U. Balthasar, C. B. Skovsted, On the edge of exceptional preservation: Insights into the role of redox state in Burgess Shale-type taphonomic windows from the Mural Formation, Alberta, Canada. *Emerg. Top. Life Sci.* **2**, 311–323 (2018).
94. B. Pratt, Preliminary biostratigraphic determinations for Middle Cambrian strata in the Dezaiko range, east-central British Columbia. Current Research, Part E, Geological Survey of Canada, Paper, 369–373 (1990).
95. S. A. F. Darroch, E. A. Sperling, T. H. Boag, R. A. Racicot, S. J. Mason, A. S. Morgan, S. Tweedt, P. Myrow, D. T. Johnston, D. H. Erwin, M. Laflamme, Biotic replacement and mass extinction of the Ediacara biota. *Proc. R. Soc. B: Biol. Sci.* **282**, 20151003 (2015).
96. J. P. Wilson, J. P. Grotzinger, W. W. Fischer, K. P. Hand, S. Jensen, A. H. Knoll, J. Abelson, J. M. Metz, N. McLoughlin, P. A. Cohen, M. M. Tice, Deep-Water incised valley deposits at the ediacaran-cambrian boundary in southern namibia contain abundant treptichnus pedum. *Palaios* **27**, 252–273 (2012).
97. C. Guan, C. Zhou, W. Wang, B. Wan, X. Yuan, Z. Chen, Fluctuation of shelf basin redox conditions in the early Ediacaran: Evidence from Lantian Formation black shales in South China. *Precambrian Res.* **245**, 1–12 (2014).
98. G.-Y. Wei, N. J. Planavsky, L. G. Tarhan, T. He, D. Wang, G. A. Shields, W. Wei, H.-F. Ling, Highly dynamic marine redox state through the Cambrian explosion highlighted by authigenic $\delta^{238}U$ records. *Earth Planet. Sci. Lett.* **544**, 116361 (2020).
99. K. Liu, Q. Feng, J. Shen, M. Khan, N. J. Planavsky, Increased productivity as a primary driver of marine anoxia in the Lower Cambrian. *Palaeogeogr. Palaeoclimatol. Palaeoecol.* **491**, 1–9 (2018).
100. C. Yang, F. T. Bowyer, D. J. Condon, X.-H. Li, M. Zhu, New U-Pb age from the Shuijingtuo Formation (Yangtze Gorges area) and its implications for the Cambrian timescale. *Palaeogeogr. Palaeoclimatol. Palaeoecol.* **616**, 111477 (2023).
101. X. Wang, X. Shi, G. Jiang, W. Zhang, New U–Pb age from the basal Niutitang Formation in South China: Implications for diachronous development and condensation of stratigraphic units across the Yangtze platform at the Ediacaran–Cambrian transition. *J. Asian Earth Sci.* **48**, 1–8 (2012).
102. Y. Zhao, J. Yuan, L. E. Babcock, Q. Guo, J. Peng, L. Yin, X. Yang, S. Peng, C. Wang, R. R. Gaines, J. Esteve, T. Tai, R. Yang, Y. Wang, H. Sun, Y. Yang, Global Standard Stratotype-Section and Point (GSSP) for the conterminous base of the Miaolingian Series and Wuliuan Stage (Cambrian) at Balang, Jianhe, Guizhou, China. *Episodes* **42**, 165–184 (2019).
103. R. R. Gaines, J. A. Mering, Y. Zhao, J. Peng, Stratigraphic and microfacies analysis of the Kaili Formation, a candidate GSSP for the Cambrian Series 2–Series 3 boundary. *Palaeogeogr. Palaeoclimatol. Palaeoecol.* **311**, 171–183 (2011).
104. J. Yao, S. Xiao, L. Yin, G. Li, X. Yuan, Basal cambrian microfossils from the yurtus and xishanblaq formations (Tarim, North-West China): Systematic revision and biostratigraphic correlation of micrhystridium-like acritarchs. *Palaeontology* **48**, 687–708 (2005).
105. R. R. Gaines, M. J. Kennedy, M. L. Droser, A new hypothesis for organic preservation of Burgess Shale taxa in the middle Cambrian Wheeler Formation, House Range, Utah. *Palaeogeogr. Palaeoclimatol. Palaeoecol.* **220**, 193–205 (2005).
106. D. E. Garson, R. R. Gaines, M. L. Droser, W. D. Liddell, A. Sappenfield, Dynamic palaeoredox and exceptional preservation in the Cambrian Spence Shale of Utah. *Lethaia* **45**, 164–177 (2012).
107. M. Webster, R. R. Gaines, N. C. Hughes, Microstratigraphy, trilobite biostratinomy, and depositional environment of the "Lower Cambrian" Ruin Wash Lagerstätte, Pioche Formation, Nevada. *Palaeogeogr. Palaeoclimatol. Palaeoecol.* **264**, 100–122 (2008).
108. G. Pari, D. E. G. Briggs, R. R. Gaines, The Parker Quarry Lagerstätte of Vermont—The first reported Burgess Shale–type fauna rediscovered. *Geology* **49**, 693–697 (2021).
109. M. Dellinger, D. S. Hardisty, N. J. Planavsky, B. C. Gill, B. Kalderon-Asael, D. Asael, T. Croissant, P. K. Swart, A. J. West, The effects of diagenesis on lithium isotope ratios of shallow marine carbonates. *Am. J. Sci.* **320**, 150–184 (2020).
110. S. M. Henrichs, W. S. Reeburgh, Anaerobic mineralization of marine sediment organic matter: Rates and the role of anaerobic processes in the oceanic carbon economy. *Geomicrobiol. J.* **5**, 191–237 (1987).
111. D. E. Canfield, Factors influencing organic carbon preservation in marine sediments. *Chem. Geol.* **114**, 315–329 (1994).
112. J. N. Betts, H. D. Holland, The oxygen content of ocean bottom waters, the burial efficiency of organic carbon, and the regulation of atmospheric oxygen. *Palaeogeogr. Palaeoclimatol. Palaeoecol.* **97**, 5–18 (1991).
113. K. M. Martin, W. T. Wood, J. J. Becker, A global prediction of seafloor sediment porosity using machine learning. *Geophys. Res. Lett.* **42**, 10640–10646 (2015).

Acknowledgment: We thank Y. Yin and Y. Lin at Nanjing University for help in elemental analysis. **Funding:** This study, as well as G.-Y.W. and F.Z., was supported by the National Key Research and Development Program of China (2021YFA0718100). G.-Y.W. and C.L. acknowledge funding from the National Natural Science Foundation of China (42192500, 42373056, 41888101, and 42130208). R.R.G. and E.A.S. acknowledge funding from the National Science Foundation (EAR-1554897 and EAR-2143164, respectively). M.Z. is funded by the Chinese Academy of Sciences (E32D530201 and XDA0430202) . K.-Q.X. acknowledges funding from the Hundred Talents Program of the Chinese Academy of Sciences. **Author contributions:** Conceptualization: G.-Y.W., M.Z., R.R.G., C.L., H.-F.L., N.J.P., and L.G.T. Investigation: G.-Y.W., B.K.-A., J.S., and C.Z. Visualization: G.-Y.W., M.Z., C.L., G.L., D.C., K.-Q.X.,

N.J.P., and L.G.T. Validation: G.-Y.W., B.K.-A., C.Z., F.Z., D.C., H.-F.L., and N.J.P. Resources: G.-Y.W., M.Z., E.A.S., R.R.G., J.S., C.L., C.Z., H.-F.L., and N.J.P. Methodology: G.-Y.W., M.Z., R.R.G., B.K.-A., and N.J.P. Data curation: G.-Y.W. Formal analysis: G.-Y.W. and G.L. Software: M.Z. Project administration: G.-Y.W., H.-F.L., N.J.P., and L.G.T. Funding acquisition: G.-Y.W., M.Z., H.-F.L., and N.J.P. Supervision: G.-Y.W., N.J.P., and L.G.T. Writing—original draft: G.-Y.W. and H.-F.L. Writing—review and editing: G.-Y.W., E.A.S., R.R.G., B.K.-A., C.L., F.Z., G.L., D.C., C.C., K.-Q.X., L.J., H.-F.L., N.J.P., and L.G.T. **Competing interests:** The authors declared that they have no competing interests. **Data and materials availability:** All data needed to evaluate the conclusions in the paper are present in the paper and/or the Supplementary Materials.

Submitted 8 August 2023
Accepted 26 February 2024
Published 29 March 2024
10.1126/sciadv.adk2152